CRACK GROWTH RESPONSE OF ALLOY 152 AND 52 WELD METALS IN SIMULATED PWR PRIMARY WATER

M. B. Toloczko and S. M. Bruemmer
Pacific Northwest National Laboratory, P.O. Box 999, Richland, WA 99352
mychailo.toloczko@pnl.gov

Abstract

The crack growth response of alloy 152 and 52 weld metals has been measured in simulated PWR primary water at both high (325-350°C) and low (50°C) temperatures. Tests were performed on samples machined from alloy 152 or 52 mockup welds. Propagation rates under cycle + hold and constant K conditions at high temperatures show stable, but extremely low SCC growth rates. The most significant intergranular cracking occurred during cycling at 50°C, particularly for the alloy 152 weld metal at high stress intensity.

I. INTRODUCTION

Alloy 690 and its weld metals are seeing increased use in many critical light-water reactor applications where they are replacing stress corrosion cracking (SCC) susceptible alloy 600 materials. A key pressurized water reactor (PWR) example is alloy 690 pressure vessel head and control-rod-drive mechanism (CRDM) feedthroughs with alloy 152 and/or alloy 52 weld metals [1-2]. These weld metals are also used as a corrosion resistant layer for alloy 600 primary water piping inlay or overlay repairs [2-4]. In most cases, tests on these weld metals have not shown any significant SCC in PWR primary water [4-6]. However, quantitative evaluations of SCC crack-growth response are extremely limited for these materials. Crack-growth-rate test results on industry-made alloy 152 and alloy 52 mockup welds are described in this paper to expand on these observations.

II. EXPERIMENTAL

Alloy 152 and 52 U-groove weld mockups produced by Mitsubishi Heavy Industries (MHI) were obtained from EPRI, and an alloy 52 butt weld mockup was obtained from AREVA NP. A brief description of the welds, their heat numbers, and compositions are listed in Table 1. Images of each of the weld mockups are shown in Figures 1-3.

Table 1. Description of weldments obtained for this study

Material - Source	Heat Numbers and Description	Composition
Alloy 152 - MHI	Filler: alloy 152, heat 307380 Butter: alloy 152, heat 307380 Description: MHI mock-up weld for Kewaunee using 304SS plate	Ni-28.7Cr-9.1Fe-0.03C-3.6Mn-0.33Si-0.15Al-0.12Ti-0.003S
Alloy 52 - MHI	Filler: alloy 52, heat NX2686JK Butter: alloy 152, heat 307380 Description: MHI mock-up weld for Kewaunee using 304SS plate	Ni-29.1Cr-10.0Fe-0.024C-0.25Mn-0.13Si-0.71Al-0.52Ti-0.01Cu-0.01Mo,<0.001S
Alloy 52 - AREVA NP	Filler: alloy 52, heat NX3926JK Butter: none used Description: Mockup butt weld using alloy 600 plate	Ni-29.1Cr-10.0Fe-0.024C-0.25Mn-0.13Si-0.71Al-0.52Ti-0.01N_2

Weld fabrication method differed for each of the weldments. For the MHI alloy 152 and alloy 52 weldments, alloy 152 (heat 307380) was buttered onto the U-groove surface for both mockups by shielded metal arc welding (SMAW). For the alloy 152 weld mockup, alloy 152 (heat 307380) was also used as the filler and was applied by SMAW. For the alloy 52 weld mockup, alloy 52 (heat NX2686JK) was used as the filler and applied by gas tungsten arc welding (GTAW). Welding parameters for the fill materials were substantially different with the alloy 152 SMAW having a deposition speed of 4-25 cm/min with a current of 95-145 A, and the alloy 52 GTAW having a deposition speed of 4-10 cm/min with a current of 150-300 A. Welding parameters for the AREVA alloy 52 weldment were not provided.

The welds were tested in the as-welded (AW) condition with the exception of one test that was performed on an MHI alloy 152 weld that had been given

a low-alloy steel (LAS), stress-relief heat treatment of 610°C/12 h followed by air cooling. Orientations of the specimens relative to the welds are shown in Figures 1-3. Before machining specimens, the blanks were etched to allow viewing the weld morphology, and a desired crack growth path through specific weld passes was determined. Specimens were machined from the blanks to target the desired crack growth path. 0.5T compact tension (CT) specimens with 5% side grooves were used for all the tests. Table 2 provides a list of specimen identification codes for each of the materials tested.

Crack growth testing was performed in recirculating water autoclave systems capable of operation up to 360°C. Flow rate through a four-liter autoclave is maintained at 200 cc/min giving approximately 3.5 autoclave water exchanges per hour. Water chemistry is maintained through a combination of a boric acid and lithium hydroxide saturated mixed bed resin demineralizer, active stock solution injection, and a continuously circulating four-liter water column used to bubble gasses through the autoclave feedwater. Active load control is obtained through the use of software that interacts with a load cell and a servoelectric load frame. Crack length is estimated in-situ using a reversing direct current potential drop (DCPD) system. Intrinsic resistivity changes of the test material at PWR water temperature is handled by a DCPD reference potential attached directly to the CT specimen. For selected experiments, a zirconia membrane reference electrode was utilized to allow corrosion potential measurement of the specimen and a Pt coupon during testing. Crack growth tests were performed with two specimens in series allowing a greater range of material conditions to be examined in a shorter period of time. Experiments were conducted in simulated PWR primary water with 1000 ppm B, 2 ppm Li and 29 cc/kg H_2 at 325 or 350°C. Limited testing was also performed at 50°C under the same primary water conditions. The stress intensity (K) was controlled to a value of 30 MPa√m under most conditions, although some specimens were evaluated at 40 MPa√m as well.

Specimens were first precracked in air followed by further crack extension using aggressive cycling in high temperature water. A variety of loading conditions were used to attempt to transition from the transgranular precrack to an intergranular (IG) SCC crack front. Loading conditions included R values ranging from 0.5 to 0.9, the addition of hold times up to 24 h, and various "periodic unload" schemes with a symmetric or a sawtooth wave form (e.g., rapid unload followed by a slow reload). No one condition was found to promote SCC engagement better than others in these SCC resistant alloys. However from a testing perspective, it is favorable to choose a cycling condition that moves the crack forward fast enough to encounter as many grain boundaries as possible while still having sufficiently gentle loading conditions to allow the crack to go IG if that is a favored path. Based on the current work and tests on alloy 690 [7], a final cycling step at 0.001 Hz with R = 0.5-0.7 was often used and followed by the addition of hold times before determining crack growth rates at constant K.

Table 2. Summary of testing details for each specimen

Specimen ID	Material	Thermomechanical Treatment
CT013	MHI alloy 152	AW
CT017	MHI alloy 152	AW + LAS heat treat
CT018	MHI alloy 152	AW
CT024	AREVA alloy 52	AW
CT025	MHI alloy 52	AW
CT032	AREVA alloy 52	AW
CT033	MHI alloy 52	AW

The response of the material during transitioning was assessed continuously by comparing current propagation rates to results from earlier tests. As the database of observed crack growth rates and accompanying crack surface morphologies from previous tests grew, higher crack growth rates during transitioning (particularly during cycle + hold loading) could be identified. If a crack growth rate during transitioning was indicative of a non-engaged crack front, then the crack would often be re-transitioned in a repeat attempt to improve SCC engagement. For these SCC resistant alloys, several transitioning attempts were typically made before documenting constant K, crack-growth-rate response.

III. RESULTS AND DISCUSSION

The first SCC crack-growth test was performed on a single CT specimen (CT013) of the MHI alloy 152 in the as-welded condition. Crack extension and transitioning were done in 325°C PWR primary water by cyclic loading at decreasing frequencies, an R value of 0.7, and a K of 30 MPa√m. After >500 h cycling at 0.001 Hz, hold times of 2.5 h and then 24 h were added as shown in Figure 4. Extremely low, but stable crack growth rates were observed under these conditions decreasing to $3x10^{-9}$ mm/s after ~1000 h for the 24 h hold. Constant K was established and the measured propagation rate gradually decreased to $<5x10^{-10}$ mm/s over the next few months. This first test was ended after ~2200 h (3 months) at constant K and the crack growth surface examined as shown in Figure 5. Local areas of IGSCC extension were found by optical imaging and scanning electron microscopy (SEM). The IG growth appeared to begin during the cycle + hold steps and the final crack front was

~35% IG. Based on this engagement, area-averaged propagation rates were determined and reported in Figure 4. If only the maximum IG crack extension was considered, estimated local rates would be ~5X higher.

The next two alloy 152 specimens were tested in series with one in the as-welded condition (CT018) and one given a LAS stress-relief heat treatment (CT017). Overall crack growth response is shown in Figure 6 with testing performed both at 350°C and at 50°C. Unlike the first test, shorter transitioning intervals were used with more emphasis on sampling the response of the material at several different regions in each specimen and on trying different methods to obtain a more engaged IG crack front. The transitioning conditions used in the first region of the specimen were the same as those in the previous test on the MHI alloy 152 (CT013). The initial crack growth during cycle + hold and constant K steps were essentially identical to that observed in the previous test (specimen CT013) as shown in Figure 7. Stable propagation rates were measured under cycling, and slowed to extremely low values ($<5x10^{-10}$ mm/s) under constant K of 32-33 MPa√m. A second region of the alloy 152 microstructure was then evaluated by extending the crack ~0.4 mm in both samples by moderate cycling. An alternate SCC transitioning approach was then used with sawtooth waveforms during cycling with R = 0.5, a 12 s unload, and increasingly longer reload time ranging from 300 s to 1000 s. After ~100 µm of growth with the 1000 s reload time, the R value was then changed to 0.7 and a 2.5 h hold was added. Over a period of ~200 h, the crack growth rate was observed to slowly decrease to a rate below $1x10^{-8}$ mm/s at a corrected K of 35 MPa√m as shown in Figure 8. The load cycle was then converted from a sawtooth waveform to a 0.001 Hz symmetric waveform while maintaining the same 2.5 h hold time and R value of 0.7. As shown in Figure 8, no change in propagation rate occurred upon converting to the symmetric waveform, and the rate of $\sim6x10^{-9}$ mm/s was slightly less than that observed when this same cycle + hold condition was used earlier in the test. Since no SCC enhancement was indicated during the cycle + hold loading, it was decided to investigate the crack growth response at a higher target K of 40 MPa√m. This was done for both specimens by extending the crack 0.4 mm using cyclic loading (0.01 Hz, R=0.6) and a dK/da value of 100 MPa√m/mm. Based on post-test correction of the crack length, the actual K value was ~48 MPa√m after the dK/da transition. After switching to 0.001 Hz (symmetric waveform) and an R of 0.7, propagation rates were evaluated after adding a 2.5 h hold and finally during constant K as shown in Figure 9. Crack growth rates were 3-4X higher than seen at lower K levels at 1.7-$2.1x10^{-8}$ mm/s and 1.0-$1.7x10^{-9}$ mm/s for the cycle + hold and constant K conditions, respectively.

The final stage of the test examined crack-growth response at 50°C while maintaining PWR primary water chemistry conditions, including a dissolved hydrogen content of 29 cc/kg. After extending the crack ~1 mm by cycling at 0.01 Hz, transitioning and constant K steps were performed as shown in Figure 10. The crack growth rates during cyclic and cycle + hold loading were found to be ~2-3X greater than rates observed at 350°C at the same stress intensity value and cycling conditions. However when the test was converted to constant K, the crack in both specimens ceased growing entirely. When cyclic loading conditions were re-established, crack growth resumed. The test was later converted to constant K, again with no crack advance. This suggests that dynamic strain during cycling is required for environment-assisted propagation at this low temperature.

One of the characteristic features of the crack growth response at 50°C was a relatively large systematic variation in the DCPD-measured crack length during low frequency cyclic loading conditions. To better assess the cause of this, the DCPD response was examined in detail during cycle + hold loading conditions as shown in Figure 11. Large spikes in the apparent crack length were found to occur at the onset of each load cycle with the crack length decaying rapidly to a value slightly higher than existed prior to the load cycle. The spikes in the crack extension are clearly not a real phenomenon, but each load cycle does produce a small increment in crack length. The lack of growth during the hold time is consistent with the lack of growth at constant K. It is thought that the spikes in crack length are due to the formation (during constant load) and destruction (during cycling) of "conducting" bridges behind the crack front. These bridges may form behind the crack front due to the electrochemical conditions of the PWR primary water at 50°C where Ni metal is stable. Enhanced electronic conduction across the crack will result in DCPD significantly underestimating the actual crack length. Dynamic deformation during load cycling is apparently sufficient to break the bridges resulting in an immediate increase in DCPD-measured crack length. However, they reform rapidly once the load cycle is complete.

As a final phase of the test, the fatigue crack growth rate of these specimens was measured in air and found to be 3-4X lower than in PWR primary water, further demonstrating that propagation at 50°C was an environment-assisted process. The specimens were then fatigue fractured in air to expose the crack growth surfaces. An optical image highlighting the crack growth surface created during high temperature testing is shown in Figure 12. Lines on the surface separate different phases of the tests. Regions of IGSCC are apparent, especially at the final high temperature crack front with the higher K level. SEM images in Figure 13 better illustrate the degree of IG engagement with the final crack front at 350°C having about 40% IG engagement. Somewhat surprisingly, more than 90% IG engagement was found to occur during the crack growth testing at

50°C. This IG growth is consistent with the higher crack growth rates observed during cycling loading of the specimens at 50°C in water.

The next test to be reviewed is the crack growth response of two alloy 52 welds, one made by AREVA (CT024) and the other made by MHI (CT025). An overview of the entire crack growth test is shown in Figure 14. The test can be broken up into three phases. The first two phases evaluated crack growth response during transitioning and constant K at 350°C at two different regions in the specimens. The third phase of the test examined the 350°C constant K crack growth response after extending the crack by cyclic loading at 50°C. This unusual transitioning method was based on the high degree of IG engagement observed in the MHI alloy 152 specimens during cyclic loading at 50°C.

In the first region that was evaluated, crack growth rates during cycle + hold loading with R = 0.7 were found to be a factor of 2-5X lower than transitioning crack growth rates in the MHI alloy 152 specimens from previous tests. Additional transitioning steps were applied using an R = 0.5 and crack growth rates increased, however propagation rates in the alloy 52 specimens remained a factor of ~2X lower than for the alloy 152 specimens under equivalent gentle cycling. Cycle + hold and constant K response was then determined as presented in Figure 15. The crack growth rate during the extended time at cycle + hold loading was very linear with no suggestion of any change in the degree of engagement. At approximately 2130 h, the loading conditions were set to constant K and propagation rates of $<5x10^{-10}$ mm/s were measured over the following ~500 h. Transitioning was reinitiated using a series of different hold times and periodic unloading steps, but none gave any indication of an increase in engagement, and it was decided to advance the crack in each specimen to a new region. Using moderate cyclic loading conditions, the crack in each specimen was advanced over 0.5 mm, and transitioning was initiated using symmetric waveforms with R = 0.5. Propagation rates during subsequent cycle + hold conditions were found to be only slightly higher ($\sim 1x10^{-8}$ mm/s) than the rates observed in the previous region suggesting that constant K crack growth rate for the specimens would again be well below $1x10^{-9}$ mm/s.

For the final phase of the test, transitioning at 50°C was performed. In an attempt to generate an engaged IG crack front in the alloy 52 specimens, it was decided to perform similar cycling at 50°C in PWR primary water as done for the alloy 152 specimens that exhibited extensive IG cracking. The crack growth response of the alloy 52 specimens at 50°C is shown in Figure 16. While an increase in propagation rate with time during 0.001 Hz step is suggestive of an improvement in engagement, the crack growth rate in each of the three cyclic steps was consistently lower than the rates observed at 350°C and much lower than measured for the alloy 152 specimens under equivalent cycling conditions. After ~1000 hours of crack extension at 50°C, the loading was converted to constant K, and the test temperature was brought back up to 350°C. DCPD fluctuations were allowed to settle out for 24 h before crack length measurements were resumed. The resulting crack length with time response at 350°C is shown in Figure 17. As can be seen, very high initial crack growth rates in excess of $1x10^{-7}$ mm/s were observed. Over the next 1400 h (2 months), the propagation rates slowly decreased reaching levels below $1x10^{-9}$ mm/s similar to earlier high-temperature constant K response for these specimens. The high initial DCPD-measured growth rates is possibly due to the disruption of conducting bridges across the cracks formed at low temperatures and during the temperature increase to 350°C. As noted previously, electrochemical conditions are very Ni-metal stable at 50°C and move closer to the Ni/NiO potential as the temperature is increased. The increase in DCPD-measured crack length may be due to oxidation or creep-induced fracture of these bridges in the crack at high temperature. It was not possible to separate this process from actual propagation, but it appears likely that the final constant K rates after 2 months are more representative of actual SCC growth rates.

The test was ended, and the specimens were fatigued open in air to document the crack growth surfaces. Optical images of the crack growth surfaces for the AREVA and MHI alloy 52 specimens are shown in Figure 18 and 19, respectively. Several distinct bands are apparent on the surface, and are labeled as A through D in Figure 18. Band A corresponds to the transitioning and constant K testing in the first region that was examined. Band B corresponds to rapid crack extension performed to move the crack front forward to the next microstructural region of crack-growth testing while C corresponds to the transitioning steps in this region. Finally, band D corresponds to crack extension at 50°C and during the subsequent constant K phase at 350°C. SEM examination determined that the crack-growth surface of the AREVA alloy 52 specimen was transgranular except for two small protrusions of IG growth within the yellow boxed region. An SEM example of this IG morphology is presented in Figure 20(a). This IG growth appears to have been initiated and propagated during 50°C cycling with no significant IG cracking produced during prior testing at 350°C. A higher fraction of IG cracking was discovered for the MHI alloy 52 specimen as indicated by the yellow boxed regions in Figure 19. Whereas the AREVA alloy 52 specimen was less than 5% IG at the final crack front, the MHI alloy 52 specimen was ~35% IG. The cracking morphology in one of these IG regions for the MHI sample is documented in Figure 20(b) and again appears to have initiated and propagated during 50°C cycling.

A key issue that remained was whether any significant IGSCC growth occurred during constant K testing at 350°C after crack extension at 50°C. In order to

better assess the effects of the temperature change on the DCPD-measured crack length, tests were performed on a second set of AREVA (CT032) and MHI (CT033) alloy 52 specimens in simulated PWR primary water. The specimens were transitioned for several weeks at 350°C and displayed similar cyclic crack growth response as specimens CT024 and CT025. The temperature was then decreased to 50°C and the crack extended by ~1 mm using cyclic loading conditions similar to what was used for the first set of alloy 52 specimens. Loading was then converted to constant K at a low value of 10 MPa√m and the temperature brought back up to 350°C. Considering the high SCC resistance of these materials, no crack growth is expected at this low K value. However, nearly identical DCPD crack growth response can be seen comparing Figure 21 (CT032/33, low K) to Figure 17 (CT024/25, high K). These new crack growth results and crack surface observations support the conclusion that slow oxidation of Ni-metal bridges is occurring in the cracks produced at 50°C, and this is reducing or removing DCPD current conduction paths behind the crack front. The very similar crack growth rates between the tests at 10 MPa√m and 30 MPa√m suggest that very little IGSCC growth occurred after returning to 350°C even with ~35% IG engagement in the MHI specimen produced by transitioning at 50°C.

IV. Summary and Conclusions

The crack growth rate response of industry-made alloy 152 and alloy 52 weld mockups was investigated in simulated PWR primary water. Several different transitioning conditions were used in each of the tests in an attempt to create an engaged IG crack front at 325-350°C. This was most successful for the MHI alloy 152 weld metal where up to ~40% IG engagement was obtained. However, average crack growth rates under constant K conditions were consistently below $1x10^{-9}$ mm/s at 30-35 MPa√m. Propagation rates increased at higher K levels, but still remained very low ($1-2x10^{-9}$ mm/s). Crack growth rate testing of the MHI and AREVA alloy 52 weld metals in 350°C water at 30 MPa√m produced no significant IG cracking. Measured propagation rates were more than 50% less than the values observed in the MHI alloy 152 during gentle cycling and cycle + hold conditions. As shown in Figure 22, propagation rates at constant K in the MHI alloy 52 were comparable to the MHI alloy 152 while the AREVA alloy 52 specimen showed little or no crack growth at constant K. Based on the crack-growth surface examinations, the alloy 152 weldment exhibits a higher susceptibility to IGSCC in 350°C water than the two alloy 52 weldments. However, it is important to reiterate that the measured SCC growth rates for the alloy 152 were low in all cases. Additional experimentation is underway on the alloy 52 weld metals to better assess 350°C crack growth response including evaluation at higher K levels.

Crack growth testing was also performed at 50°C in simulated PWR primary water in some of the specimens. The MHI alloy 152 tested at 48 MPa√m was found to be very susceptible to IG cracking during cyclic loading at 50°C, having a final crack front that was ~90% IG. Propagation rates under cyclic and cycle + hold loading conditions were 2-3x greater at 50°C than equivalent loading conditions at 350°C. No crack extension was observed at constant K loading at 50°C suggesting that dynamic strain at the crack tip during cycling is required for what is likely hydrogen-assisted crack growth at this low temperature. The MHI alloy 52 weld metal was also found to be more susceptible to IG cracking at 50°C than at 350°C. An ~35% IG crack front was obtained during cyclic loading at 50°C and 30-33 MPa√m. Despite this IG cracking, measured crack growth rates at 50°C were equal or somewhat less than values observed at 350°C. Similar differences in cyclic propagations rates were found for the AREVA alloy 52 with rates at 50°C about 50% less than the rates at 350°C. Contrary to the other weldments, only isolated IG cracking was seen for the AREVA alloy 52 during cycling at ~30-33 MPa√m in 50°C water. Tests are ongoing to help determine why the alloy 52 weldments did not show the same susceptibility to IG cracking as the alloy 152 weldment at 50°C. One possible reason is the higher K and ΔK levels used for the alloy 152 that influence the magnitude of dynamic stain during cyclic loading.

In an attempt to improve IG engagement, crack extension was produced at 50°C in the alloy 52 weld specimens, and the test was then set to constant K and the temperature brought up to 350°C. DCPD-measured crack growth rates were initially quite high and decayed with time to low values over several months. Nearly identical DCPD response was observed at very low K and at 30 MPa√m indicating that the initial changes at 350°C were due to slow oxidation of conducting paths across the crack behind the crack front. Even though the MHI alloy 52 exhibited ~35% IG engagement at 50°C, subsequent IGSCC propagation at 350°C appears to be quite limited. This supports the conclusion that the high-Cr alloy 52 weld metals have excellent SCC resistance in high-temperature PWR primary water.

Acknowledgements

This research was supported by the Office of Nuclear Regulatory Research, U.S. Nuclear Regulatory Commission under Contract DE-AC06-76RLO 1830. Pacific Northwest National Laboratory is operated for the U.S. Department of Energy by Battelle Memorial Institute. Technical assistance of Rob Seffens and Ruby Ermi are recognized. Special thanks are given to Al

McIlree, Greg Fredrick and Peter Scott for supplying the weld mockups for testing, and to Peter Andresen for helpful discussions concerning SCC results.

References

1. M.R. Robinson, M.L. Arey, Jr., D.E. Whitaker, S. Fyfitch, "Recent CRDM Nozzle PWSCC Experience at Oconee Nuclear Station", *5th International Symposium on Contribution of Materials Investigation to the Resolution of Problems Encountered in Pressurized Water Reactors (Fontevraud 5)*, CD-ROM, Fontevraud, France, September 23–27, 2002, Paper No. 24.
2. W. Bamford and J. Hall, "Cracking of Alloy 600 Nozzles and Welds in PWRs: Review of Cracking Events and Repair Service Experience", *Proc. 12th Int. Conf. Environmental Degradation of Materials in Nuclear Power Systems – Water Reactors*, CD-ROM, Salt Lake City, USA, August 14-18, TMS, 2005.
3. G.V. Rao, R.J. Jacko, A.R. McIlree, "An Assessment of the CRDM Alloy 600 Reactor Vessel Head Penetration PWSCC Remedial Techniques", *5th International Symposium on Contribution of Materials Investigation to the Resolution of Problems Encountered in Pressurized Water Reactors (Fontevraud 5)*, CD-ROM, Fontevraud, France, September 23–27, 2002, Paper No. 23.
4. F. Vaillant, J.-M. Boursier, L. Legras, B. Yrieix, E. Lemaire, J. Champredonde, C. Amzallag, "A Review of Weldability and SCC Behaviours of Ni-Base Weld Metals in Laboratory PWR Environment", *Proc. 13th Int. Conf. Environmental Degradation of Materials in Nuclear Power Systems – Water Reactors,* Whistler, B. C., Canadian Nuclear Society, 2007.
5. P. L. Andresen, M. M. Morra, J. Hickling, A. Ahluwalia and J. Wilson, "PWSCC of Alloys 690, 52 and 152," *Proc. 13th Int. Conf. Environmental Degradation of Materials in Nuclear Power Systems – Water Reactors,* Whistler, B. C., Canadian Nuclear Society, 2007.
6. B. Alexandreanu, "The Stress Corrosion Cracking Behavior of Alloys 690 and 152 Weld in a PWR Environment," these proceedings.
7. M. B. Toloczko and S. M. Bruemmer, "Crack-Growth Response of Alloy 690 in Simulated PWR Primary Water," these proceedings.

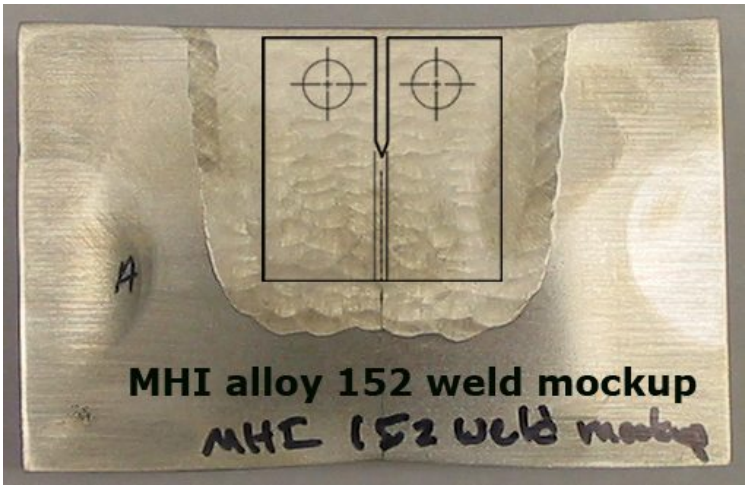

Figure 1. Image of MHI alloy 152 weld showing positioning of 0.5T CT specimens.

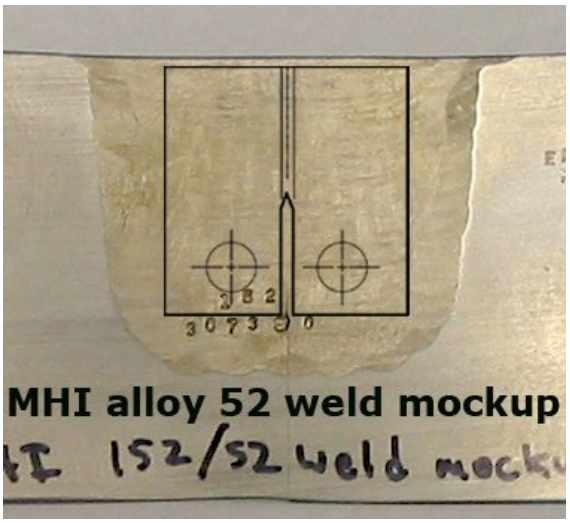

Figure 2. Image of the MHI alloy 52 weld showing positioning of 0.5T CT specimens.

Figure 3. Image of the AREVA alloy 52 weld showing positioning of 0.5T CT specimens.

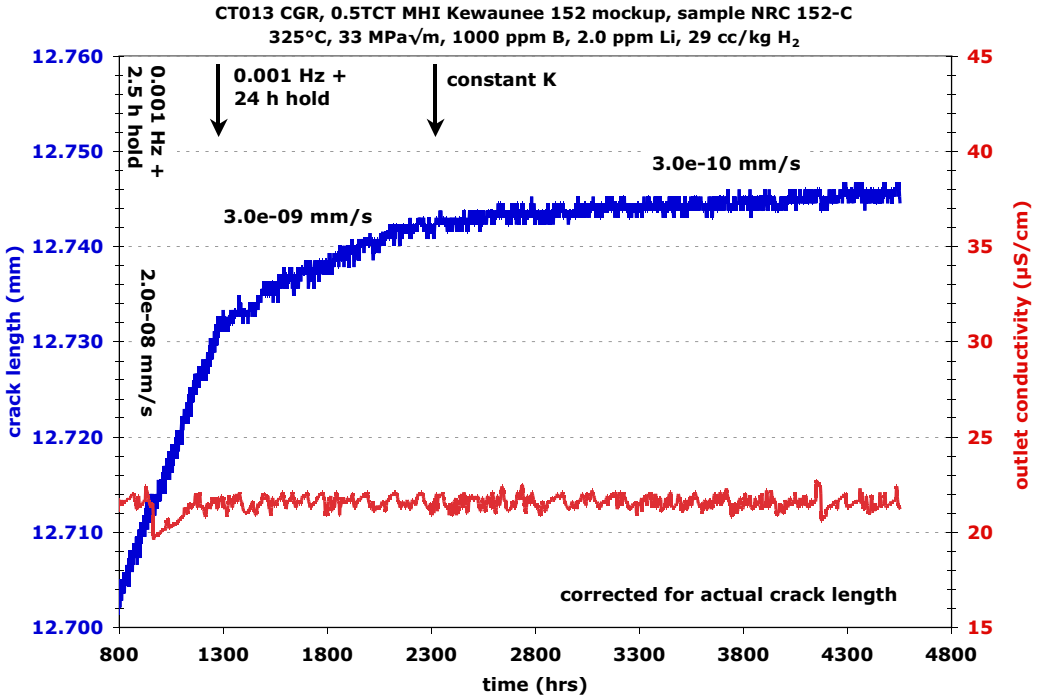

Figure 4. Crack growth response of MHI alloy 152 specimen CT013 during transitioning and constant K steps.

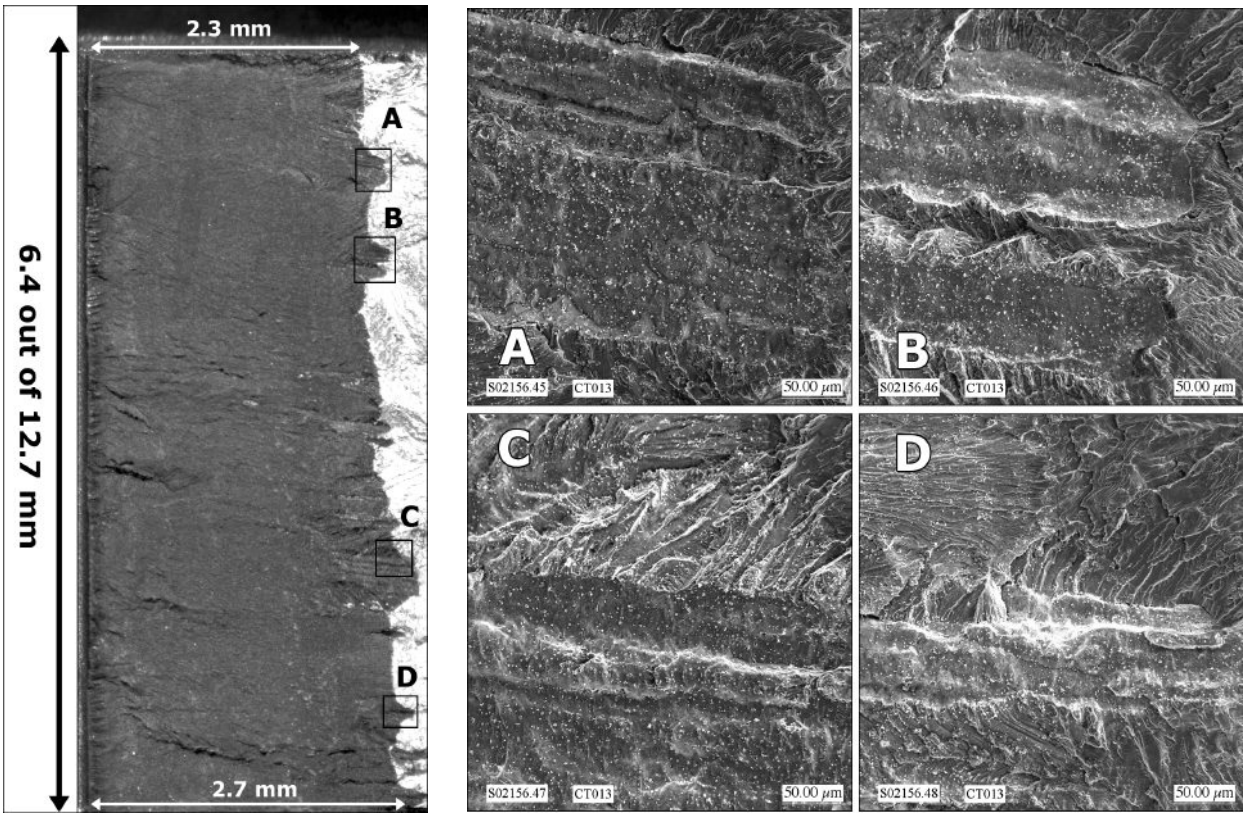

Figure 5. Crack growth surface of MHI alloy 152 specimen CT013. Optical image on left reveals local areas of SCC propagation and SEM images on right illustrate IG morphology.

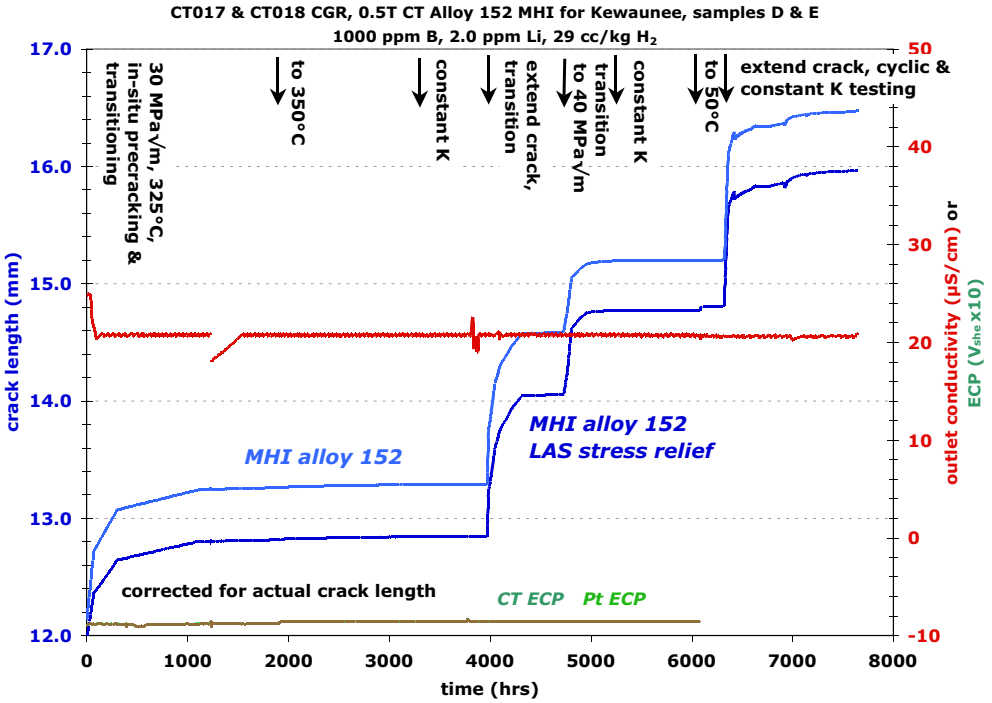

Figure 6. Overall crack growth response of MHI alloy 152 specimens CT017 and CT018.

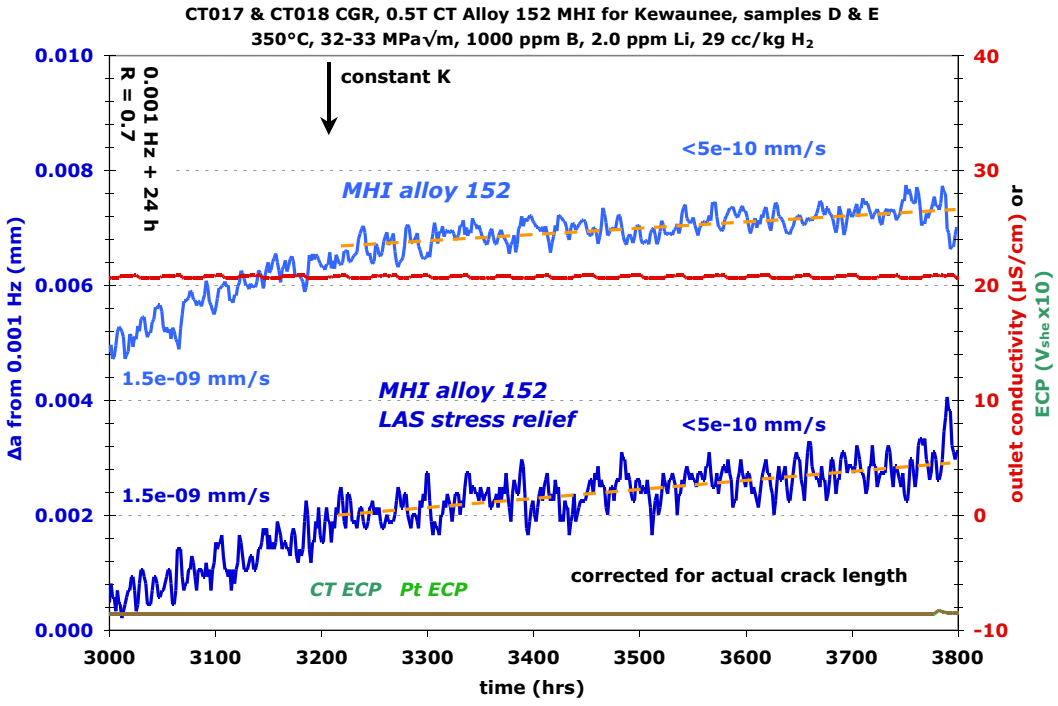

Figure 7. Constant K crack growth response of MHI alloy 152 specimens CT017 and CT018 at 30 MPa√m.

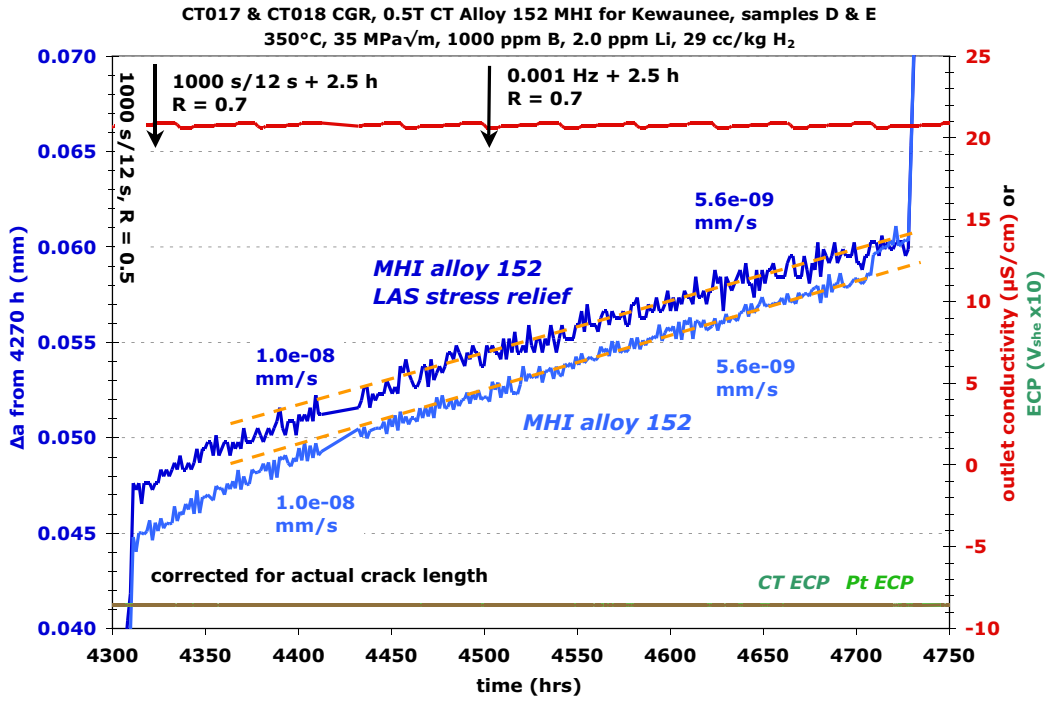

Figure 8. Crack growth response during cyclic loading conditions of MHI alloy 152 specimens CT017 and CT018 at ~33 MPa√m in the second microstructural region that was examined.

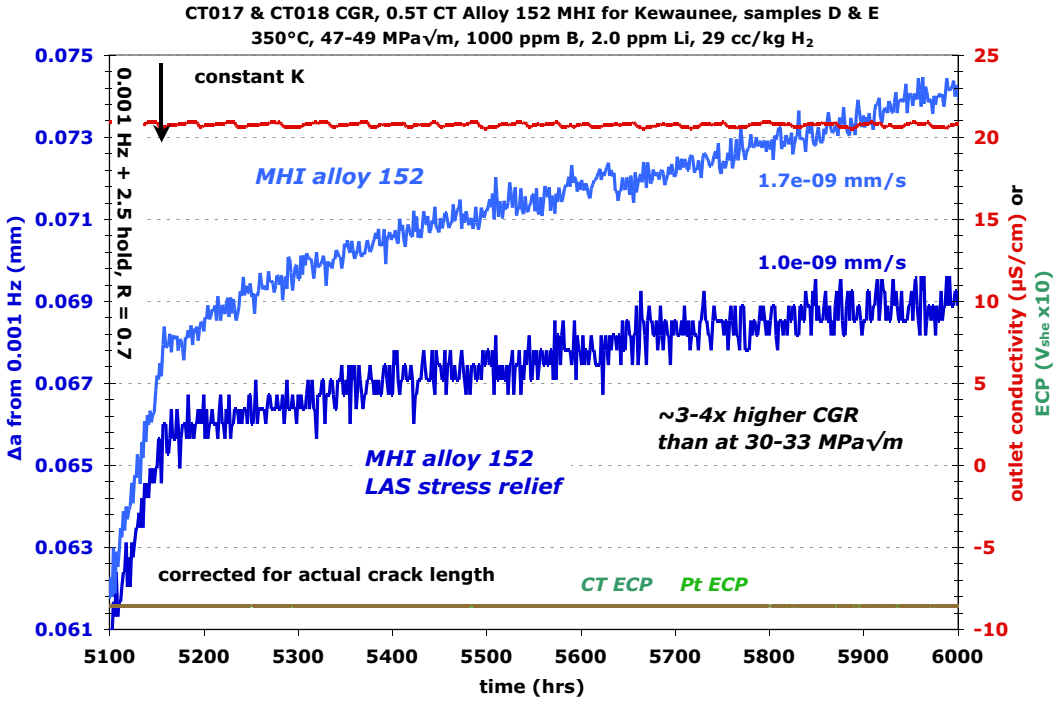

Figure 9. Constant K crack growth response of MHI alloy 152 specimens CT017 and CT018 at ~48 MPa√m.

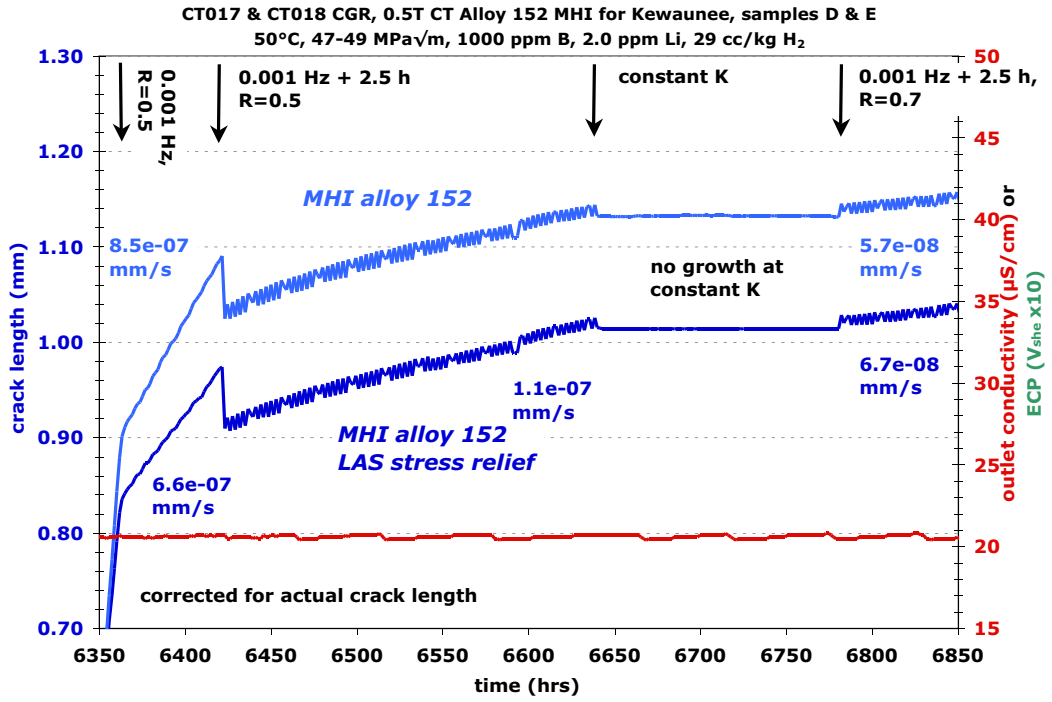

Figure 10. Crack growth response of MHI alloy 152 specimens CT017 and CT018 at 50°C in simulated PWR primary water.

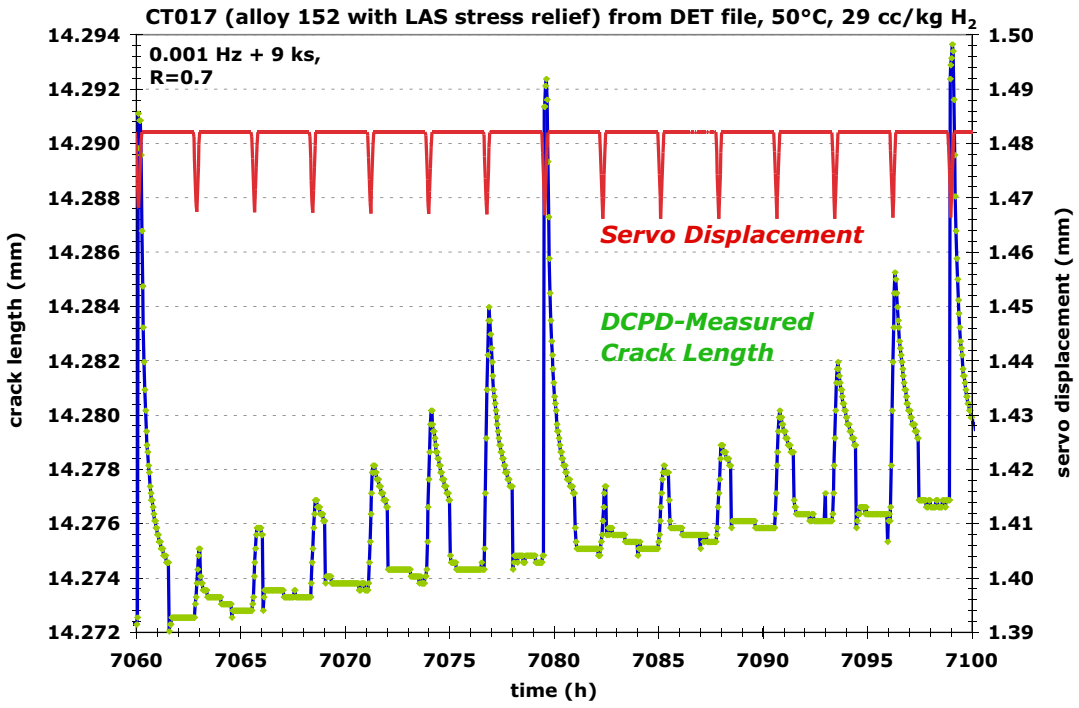

Figure 11. Detail plot showing DCPD measured crack growth response during cycle + hold loading conditions at 50°C in MHI alloy 152 specimen CT017.

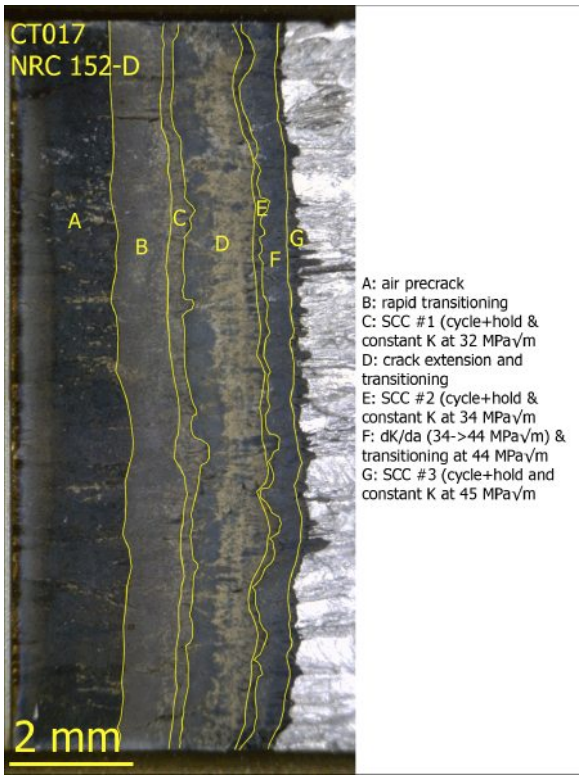

Figure 12. Optical image of high temperature crack growth surface of the MHI alloy 152 specimen CT017.

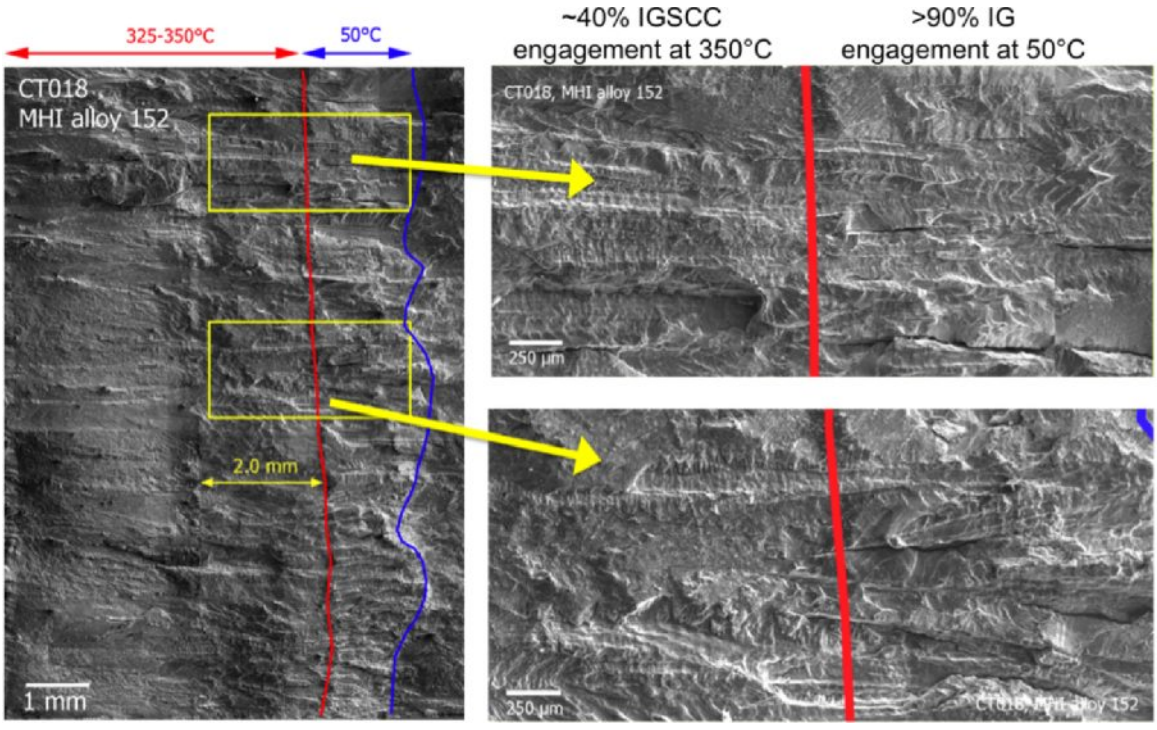

Figure 13. SEM images of 350°C and 50°C crack growth surfaces in MHI alloy 152 specimen CT018.

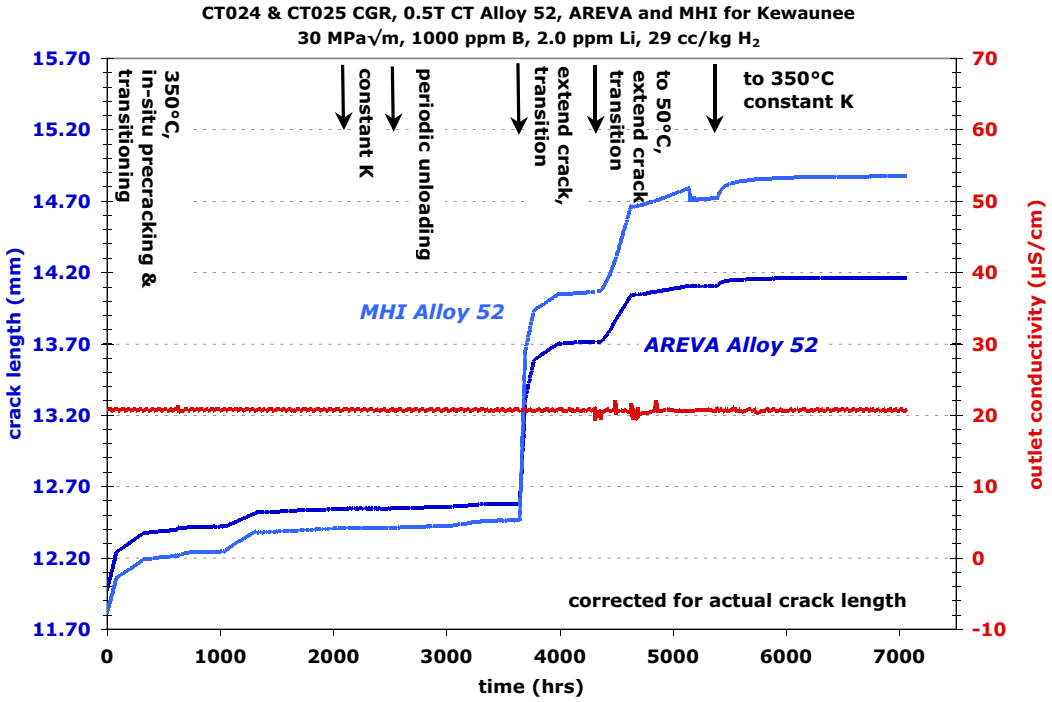

Figure 14. Overview of the crack growth response of two alloy 52 welds, one made by AREVA (CT024) and one made by MHI (CT025).

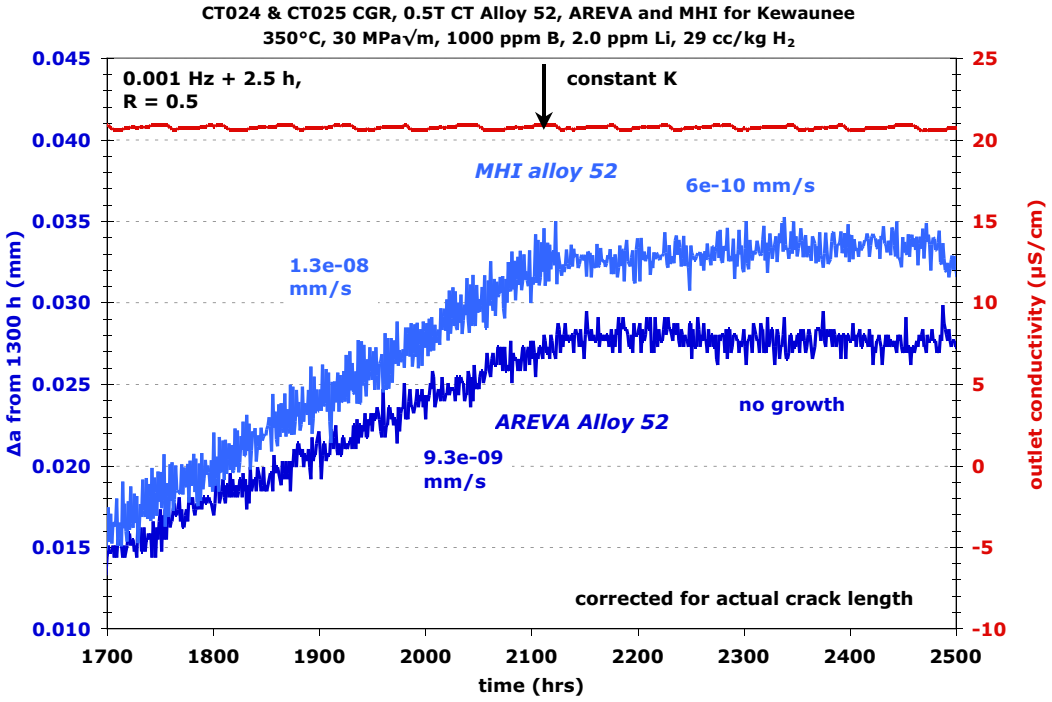

Figure 15. Cycle + hold and constant K response of the MHI and AREVA alloy 52 specimens (CT024 and CT025) in the second region of each specimen that was examined.

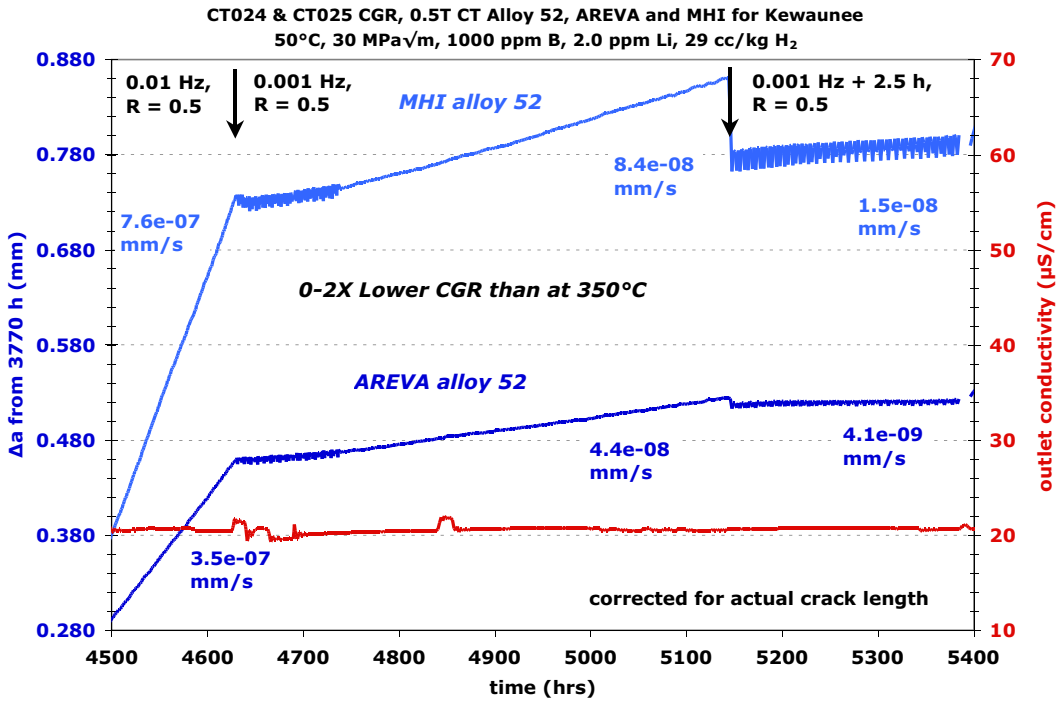

Figure 16. Overview of the crack growth response of the MHI and AREVA alloy 52 specimens (CT024 and CT025) during cyclic loading conditions at 50°C.

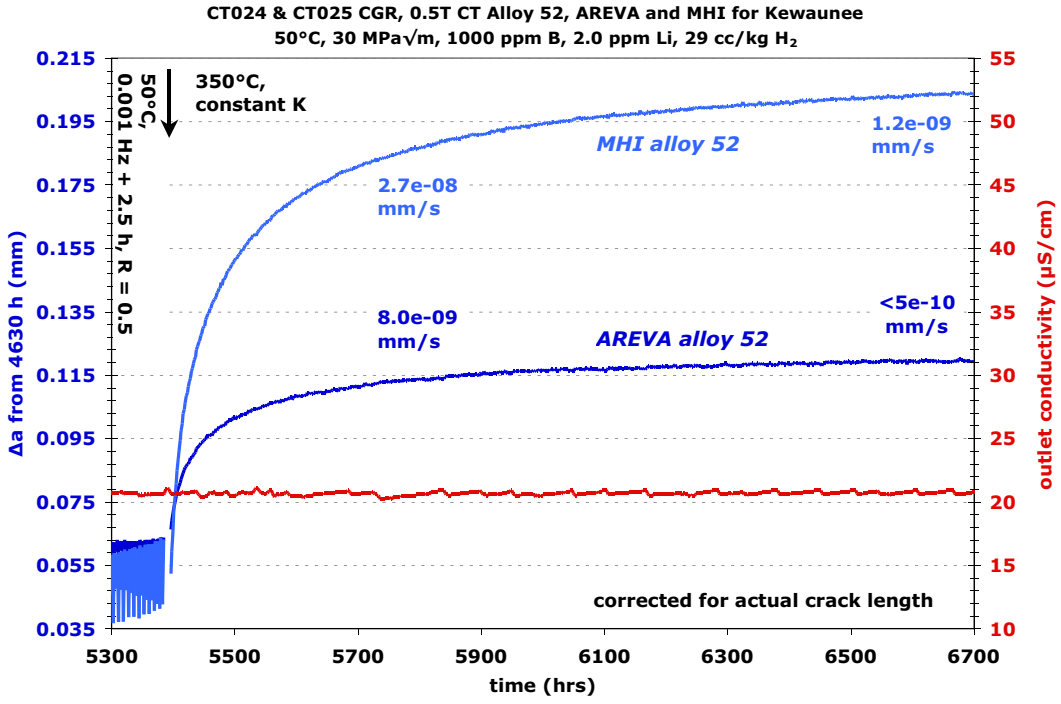

Figure 17. Constant K crack growth response of the MHI and AREVA alloy 52 specimens (CT024 and CT025) at 350°C after cyclic loading crack extension at 50°C.

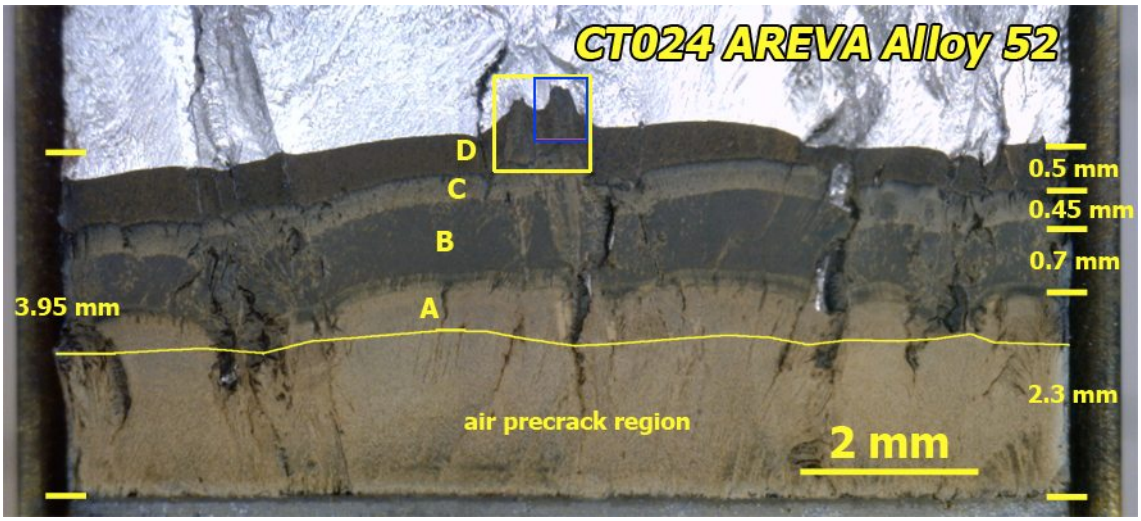

Figure 18. Optical image of the crack growth surface of the AREVA alloy 52 specimen (CT024). Four distinct bands are apparent after the air precrack boundary. The only region of intergranular growth is indicated by the yellow box. Blue box represents the area of the SEM image shown in Figure 20.

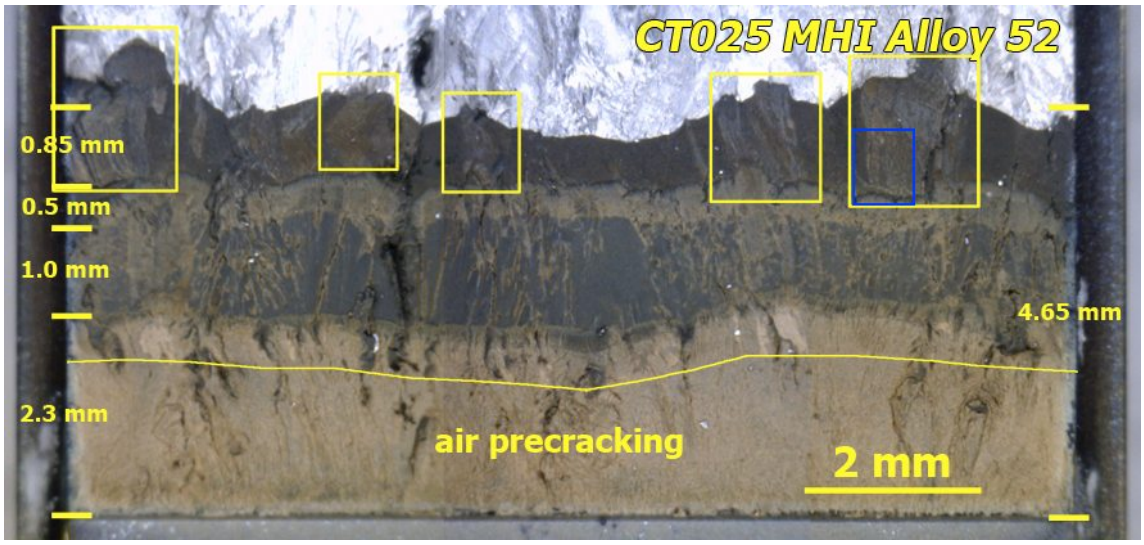

Figure 19. Optical image of the crack growth surface of the MHI alloy 52 specimen (CT025). Yellow boxes indicate regions of intergranular growth. Blue box represents the area of the SEM image shown in Figure 20.

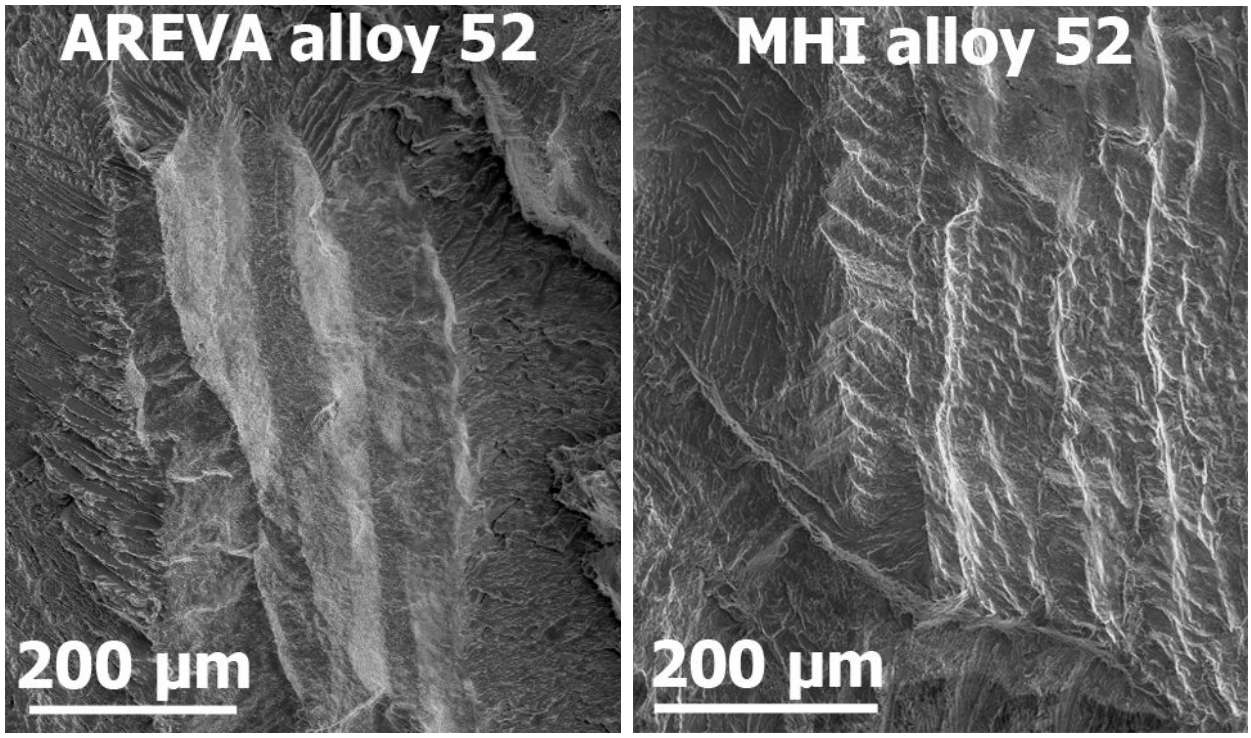

(a) (b)

Figure 20. SEM images illustrating IG regions on the crack growth surface for the alloy 52 specimens: (a) isolated IG finger-like area in AREVA sample and (b) typical IG area in MHI sample. For both specimens, some IG cracking was initiated during final growth at 350°C and continued during cycling at 50°C.

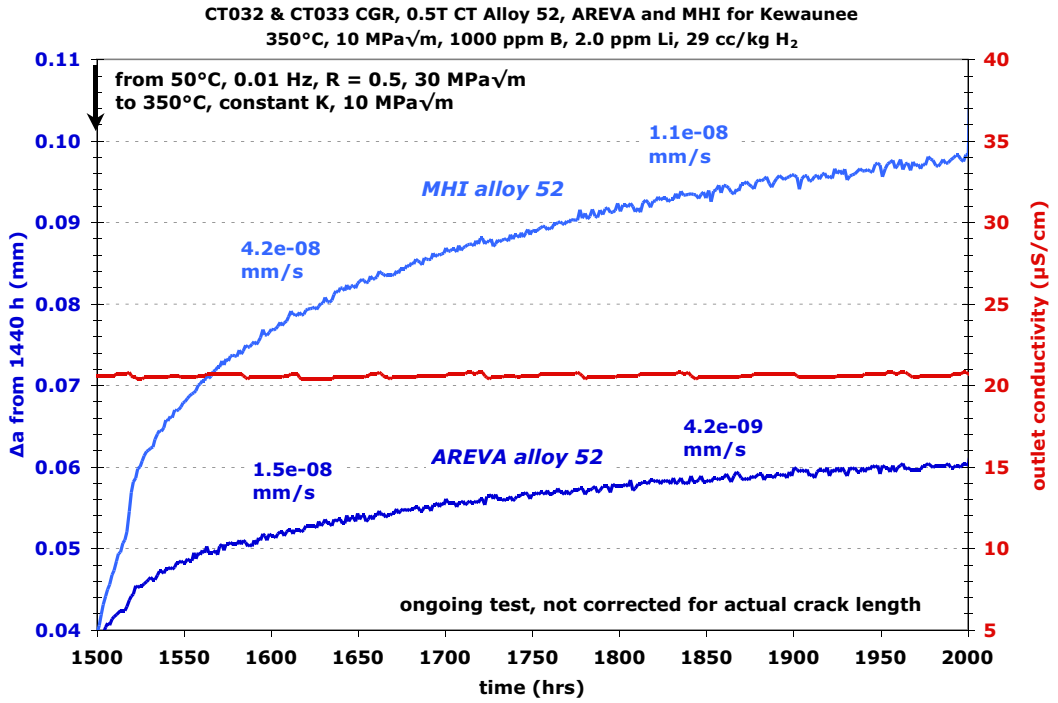

Figure 21. Crack growth response of a second set of AREVA and MHI 52 specimens (CT032 and CT033) tested at 350°C following crack extension at 50°C. Despite the low K value of 10 MPa√m, crack growth response is nearly identical to the previous test at 30 MPa√m.

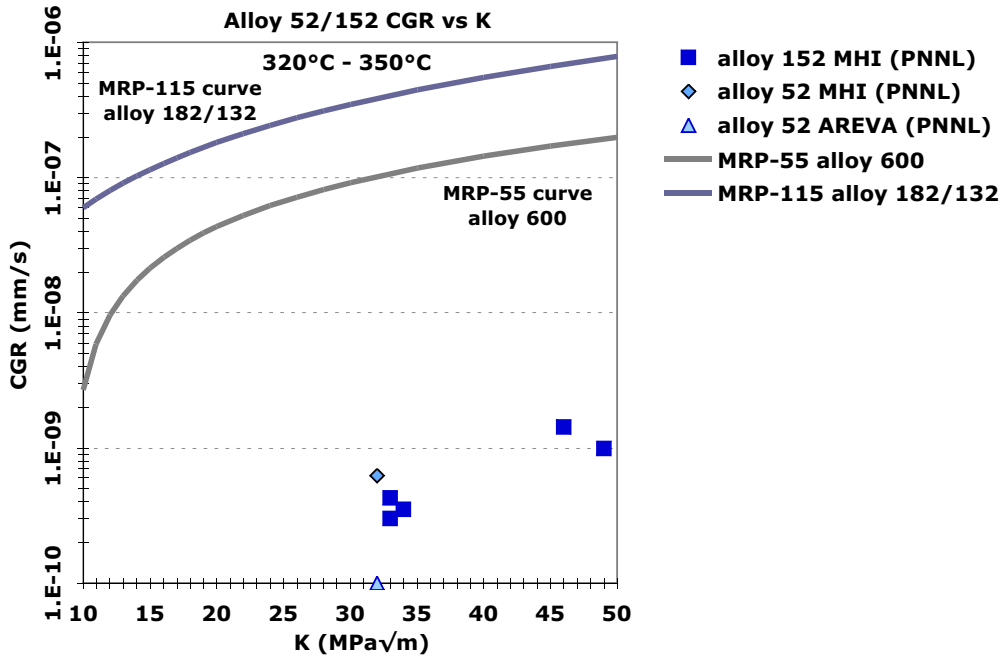

Figure 22. Crack growth rate vs K for alloy 152 and alloy 52 tests performed at PNNL.